Research Article

Multiple random phosphorylations provide long delays and switches in circadian clocks

Abhishek Upadhyay [1]*, Daniela Marzoll [2], Axel Diernfellner [2], Michael Brunner [2] and Hanspeter Herzel [1,*]

[1] Institute for Theoretical Biology, Charité – Universitätsmedizin Berlin and Humboldt University of Berlin, Philippstr. 13, 10115, Berlin, Germany; abhishek.upadhyay@charite.de, hans-peter.herzel@charite.de

[2] Biochemistry Center, University of Heidelberg, Im Neuenheimer Feld 328, 69120, Heidelberg, Germany; daniela.marzoll@bzh.uni-heidelberg.de, axel.diernfellner@bzh.uni-heidelberg.de, michael.brunner@bzh.uni-heidelberg.de

* Correspondence: abhibiotechnologist@gmail.com, h.herzel@biologie.hu-berlin.de; Tel.: +4930 2093 98402

Version June 7, 2020 submitted to Journal Not Specified

Abstract:
Theory predicts that self-sustained oscillations require robust delays and nonlinearities (ultrasensitivity). We study the circadian rhythms in the filamentous fungus *Neurospora crassa* (wild type period 22.5 hours) to investigate the underlying clock mechanisms. Its transcription translation feedback loop (TTFL) includes the activator White Collar Complex (WCC), the inhibitory FFC complex, and Casein kinase 1a. Moreover, there are multiple phosphorylation sites on FRQ (around 100) and WCC (approximately 95). A phosphoswitch controls the activity status of the FFC complex. We investigate how multiple, slow and random phosphorylations govern delay and nonlinearity in a negative feedback. We model FRQ phosphorylations with turnover of FRQ and CK1a using ordinary differential equations. Our model helps to understand the underlying mechanisms leading to delays and ultrasensitivity. The model shows temporal and steady state switches for the free kinase and phosphorylated FRQ. We show that random phosphorylations and sequestration mechanisms allow high Hill coefficients required for self-sustained oscillations. Our conceptual models help to understand multiple phosphorylations dynamics and to elucidate mechanisms of delayed switch generation.

Keywords: multiple phosphorylation; ultrasensitivity; *Neurospora crassa*, modelling; circadian clock

1. Introduction

Life on earth in forms of cyanobacteria, algae, fungi, plants and animals has evolved 24 hour periodicities called circadian clocks. This helps them to anticipate rhythmic environmental cues such as light, temperature and nutrients [1–6]. Circadian clocks regulate a wide variety of molecular and physiological processes [7–10].

Circadian oscillators are based on a transcription-translation feedback loops (TTFLs). A delayed negative feedback loop is central to the gene regulatory network [11–13]. For example, the negative feedback loop of the fungal clock is made up of the negative element (FREQUENCY [FRQ], which inhibits its own expression. The FRQ is an intrinsically disordered protein (IDP) phosphorylated by CK1a (casein kinase 1a). Later the transcription activator WCC reinitiates the cycle [14]. This design principle is conserved in other frequently used model systems. Fruit flies and animal clocks are also made up of the inhibitors, kinases and transcriptional activators. In mammalian clocks, PERIOD proteins [PER1, PER2, PER3], and CRYPTOCHROME proteins [CRY1, CRY2]) inhibit their own expression. PER2 is also an IDP as FRQ and is phosphorylated by CK1. BMAL1 and CLOCK are heterodimeric transcriptional activators [15–18].

Recent experiments suggest that many sites on both FRQ (about 100 sites) and PER2 (about 60 sites) are phosphorylated over the course of many hours at seemingly random manner [19–22]. Moreover their respective activators also get phosphorylated [15,23,24]. Phosphorylations govern nuclear translocation [25], complex formations [26,27], inactivation of transcription and stability [28,29].

We study clock mechanisms in the filamentous fungus *Neurospora crassa*. The core clock gene *Frequency* (frq) makes its product FRQ [30]. Then FRQ assembles with Frequency-interacting Helicase (FRH) and CK1a forming the FFC complex. FRQ undergoes slow, seemingly random multiple phosphorylations by CK1a [19,31–33]. FFC inactivates the WCC-induced transcription leading to a wild-type period of 22.5 hours [28,34]. Thus the TTFL is controlled by multile random phosphorylations [24,35,36].

Oscillator theory predicts that self-sustained circadian clocks require long delays and nonlinearities such as switches [37,38]. This raises two theoretical questions: (1) How can multiple random phosphorylations produce long delays? (2) What are the underlying switch mechanisms?

According to mathematical theory a delay of negative feedback loops governs the period [37,39]. Under quite general assumptions the delay is in the range between a 1/4 and 1/2 of the oscillator period [40,41]. If gene expression and inhibitor formation last about an hour, periods of 2 to 4 hours can be expected. Indeed, several TTFLs exhibit periods of a few hours including somite formation [42], NF-kB rhythms [43,44] and p53 pulses [45]. Circadian rhythms have much longer periods of about 24 hours. This implies that the associate delays last at least 6 hours. Several processes like transcription, translation, nuclear transport, post-translational modifications, mRNA decay, and proteasomal degradation may contribute to the needed delay in circadian rhythms [15,25]. It has been suggested that also the multiple phosphorylations contribute significantly to the required delay [46,47].

In order to generate self-sustained rhythms ("limit cycles") nonlinearities are necessary in addition to delays [48,49]. In many models switch-like inhibitions are postulated [50,51]. Here we explore how multiple random phosphorylation contribute to the generation of switch-like behaviour.

Fig 1 depicts the assumptions underlying our modelling approach: There is clear experimental evidence for a slow and random phosphorylation of the FRQ protein by CK1a [19,52]. Recent data suggest that an overcritical phosphorylation of the FFC complex leads to its sudden inactivation (dashed line in Fig 1). We explore how models of multiple random phosphorylations can reproduce long robust delays and switch-like behaviour.

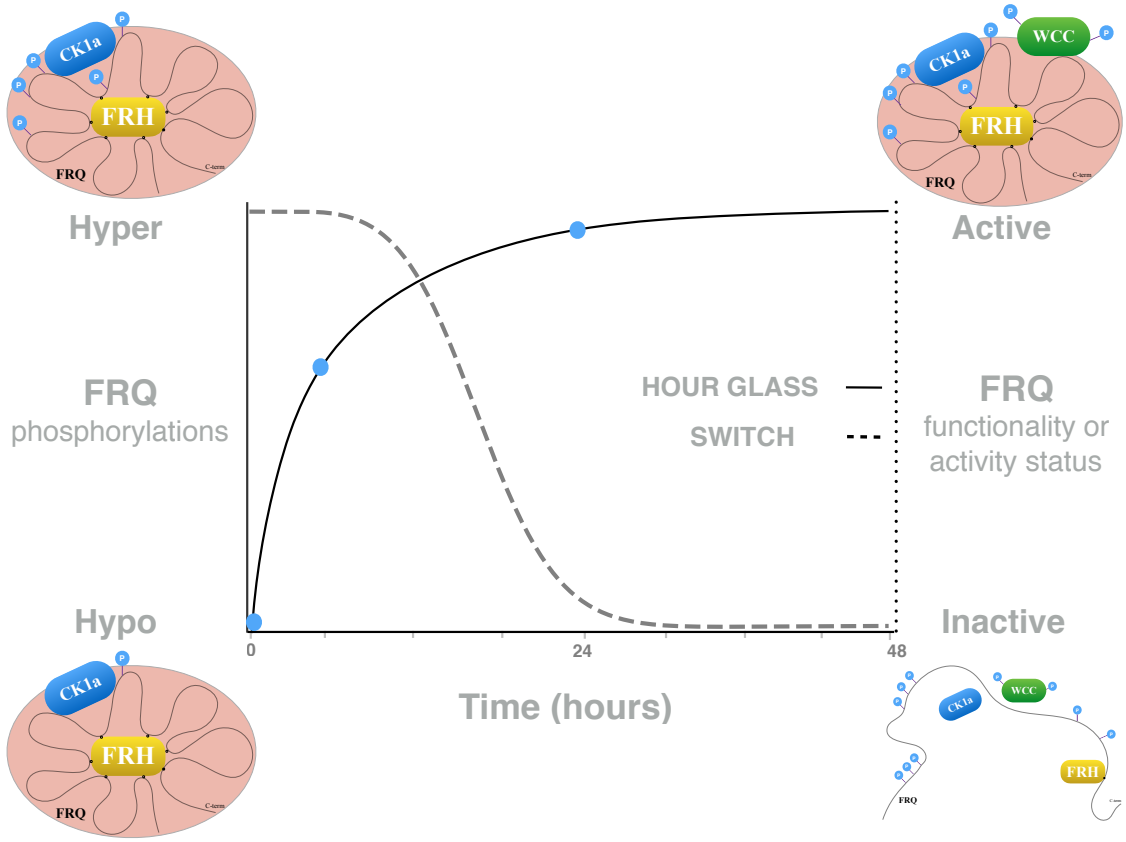

Figure 1. Phosphorylation hourglass and activity switch in the *Neurospora* clock: The FRQ protein undergoes multiple phosphorylations. Phosphorylations at 3 time-points (0, 6, 24 hours) represent recent experiments [19,52] and suggest a slow and saturated phosphorylation as shown in A6. A phosphoswitch governs the activity status of the FFC complex. The dashed line represents the simulated switch induced by hyperphosphorylated FRQ (compare Fig 7).

2. Results

2.1. Linear processive phosphorylations provides delays

The frequency gene (frq) is the core element of the circadian clock of *Neurospora crassa*. Expression of frq is controlled by the transcriptional activator WCC. FRQ is slowly hyperphosphorylated, inactivated and degraded [5,14,24]. Around 100 phosphorylation sites in FRQ have been identified. Considering that FRQ (989 amino acids) contains 132 seryl (S) and 56 threonyl (T) residues, more than 50 percent of potential sites have been found to be phosphorylated using stable isotope labeling and mass spectrometry [29,53]. Most of the CK1a sites in FRQ protein are non-consensus motifs. Recent *in vitro* and *in vivo* experiments show that about 100 sites are phosphorylated over more than a circadian day (about 48 hours) in a seemingly random manner [19]. However the detailed functions of increasing phosphorylation levels in circadian timekeeping are not well understood.

We introduce conceptual models of multiple phosphorylations. We start for simplicity with just 4 phosphorylation sites. In A1 we show the corresponding reaction scheme and the associated linear differential equations describing the FRQ turnover and processive phosphorylation. We do not explicitly consider phosphatases throughout. Phosphatases are found to be permanently available in cells and it is basically the ratio of kinase and phosphatase which takes the reaction forward [54]. Recent evidence also suggests that phosphatase play minor role in FRQ phosphorylations [55]. Fig 2 shows the increasing levels of different phosphorylations in the linear model. Note that we introduce just two parameters: a production

and phosphorylation rate k and a degradation rate kd. We have chosen parameter values that reproduce the measured full phosphorylation after about 48 hours. [19,52]. Thus we can focus on delays, amplitudes and waveforms quantified by fits of Hill-functions (see section 4.2 Materials and methods)

The curves for unphosphorylated to hyperphosphorylated FRQ exhibited delays and an accumulation of fully phosphorylated FRQ in a switch-like manner (Fig 2). Therefore even linear phosphorylations alone can provide delays. A delayed switch based on multiple phosphorylations can serve as the basic hourglass mechanism hypothesized in Fig 1. Note, that these steps required no explicit nonlinearity in the model.

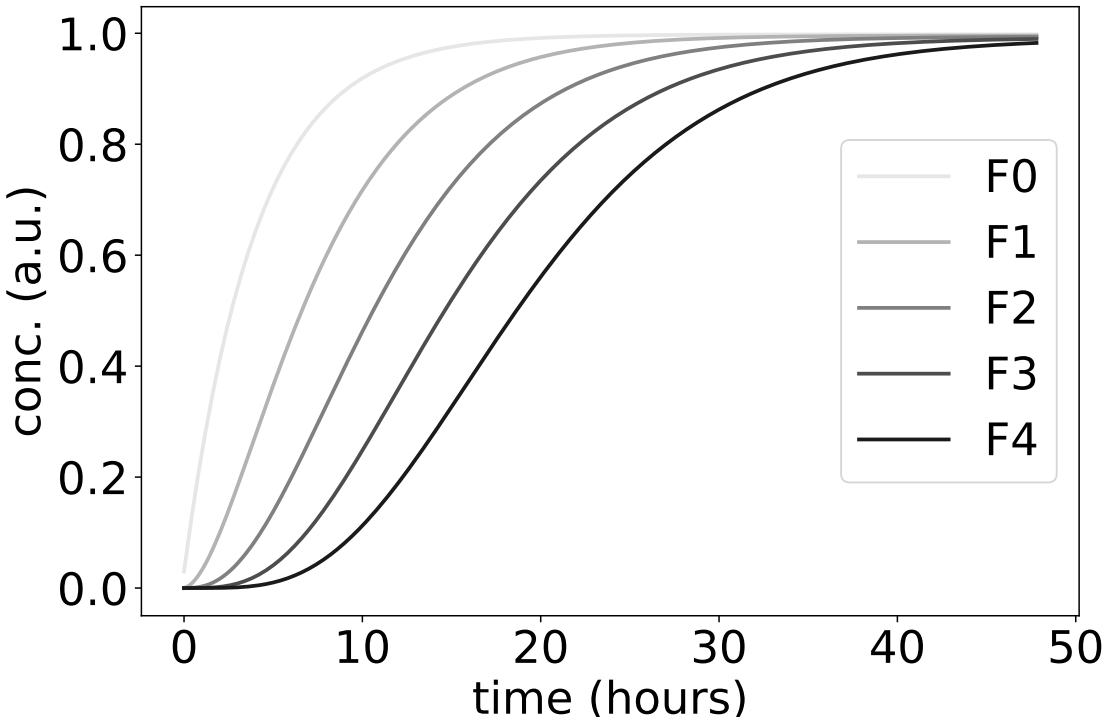

Figure 2. Modeling a delayed switch based on multiple phosphorylations: The simulations start with unphosphorylated FRQ protein. The normalized total number of FRQ with k=1,..,4 phosphorylations increases with time delays and hyperphosphorylated species (such as n = 4) accumulate in an ultrasensitive, switch-like manner.

2.2. Nonlinear models of distributive phosphorylations enhance ultrasensitivity

Kinases bind to substrates and could phosphorylate sites while staying bound (processive mechanism). Alternatively, the kinase may bind and unbind, so that next phosphorylation first requires rebinding of a kinase molecule (distributive mechanism) [54]. Distributive enzyme kinetics may lead to ultrasensitive responses in protein phosphorylations [56,57]. Note that in these studies ultrasensitivity is quantified using input-output relations. Typically steady states of phosphorylation levels are studied as a function of ligand concentrations or kinase levels. Motivated by our temporal switch in Fig 1, we focus on the ultrasensitive increase of phosphorylation with time. In this section we include production and degradation of CK1a and protein-enzyme complex formations in order to study the role of enzyme sequestration.

A2 shows the turnover of FRQ, free CK1a and bound CK1a with FRQ (FkC complexes). FRQ is sequentially phosphorylated via free kinase molecules. Using mass-action kinetics, this scheme is directly translated into a system of nonlinear ordinary differential equations (ODEs) [58–60]. The equations describe 10 time-varying concentrations of (phosphorylated) FRQ, complexes with the kinase and turnover of CK1a. The 5 kinetic

parameters in the ODEs are enumerated as Pp and Pc, k1, k2 and kd (see A2) respectively for production of protein and kinase, rates of phosphorylation and degradation.

Fig 3 shows the production and phosphorylation of FRQ and CK1a starting at zero levels. F0 denotes the unphosphorylated FRQ protein whereas F1, F2, F3, F4 represent increasing phosphorylation levels. Ct and Cf denote the amounts of total and free CK1a respectively. The phosphorylated FRQs show sigmoidal changes in its concentrations together with the expected delays. There is an initial sharp peak of free enzyme but later most of the enzyme is bound in protein-enzyme complexes ("sequestered"). A5 shows the Hill coefficients for phosphorylated FRQs (F0...F4) calculated along the lines of [61,62]. In comparison to linear phosphorylations shown in Fig 2, nonlinear phosphorylations provide higher Hill coefficients. Note, however, that the amplitudes decrease drastically for higher phosphorylation levels.

Our simulations start at low levels of FRQ and CK1a. This protocol allows to analyze large ranges of substrate and enzyme levels. In vivo, however, the enzyme CK1a is permanently present.

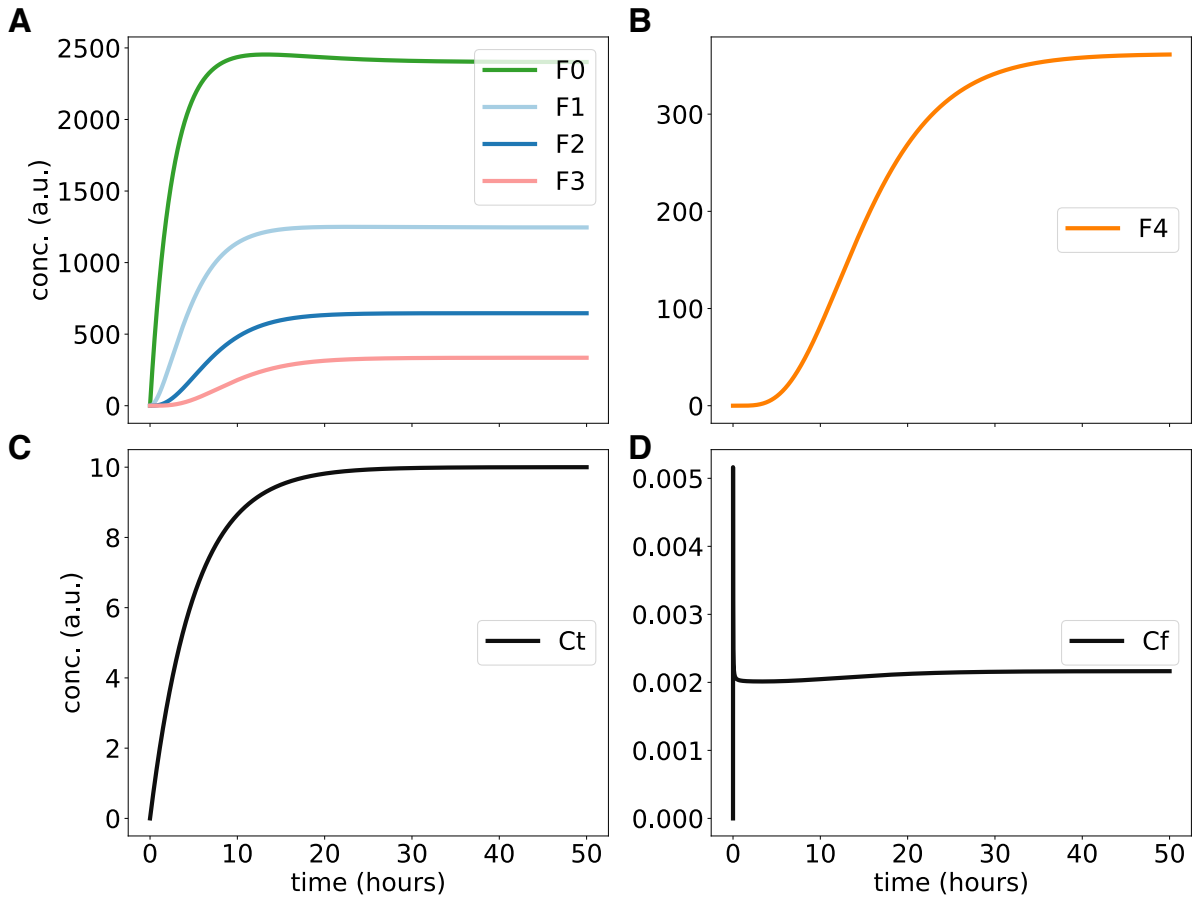

Figure 3. Kinetics of nonlinear distributive phosphorylations: (A) and (B) show steep curves of hypo- and hyper-phosphorylated FRQ proteins over time. Graph (C) and (D) display total and free kinase concentrations, respectively.

2.3. Sequestration generates threshold behaviour

It was shown in the preceding section that sequestration can enhance switch-like behaviour. In Fig 3, the amount of available CK1a was relatively small compared to FRQ and thus most of the enzyme was sequestered. It is known, however, that CK1a levels are quite high in *Neurospora* [14]. Consequently, we study here the effects of enlarged kinase production Pc. It turns out that higher CK1a levels lead to a sharp threshold.

In Fig 4 the levels of phosphorylated FRQ proteins F1, F2, and F3 increase initially as in Fig 3. After about 10 hours, however, they decay to quite small values. In parallel, the fully phosphorylated FRQ protein F4 reaches high levels (see upper right graph in Fig 4). If full phosphorylation reaches saturation the amount of free kinase is increasing suddenly. Magnifications reveal that the apparent "kinks" in the time-courses are smooth curves (see A7).

In summary, for higher CK1a levels threshold behaviour arises reflecting the sequestration of enzymes by different species of phosphorylated FRQ proteins. Note, that the initial sharp increase of free FRQ levels is based on our somewhat artificial initial condition of zero CK1a levels. In vivo the equilibrium between free and bound FRQ (compare also A7) is reached more quickly due to the omnipresence of CK1a.

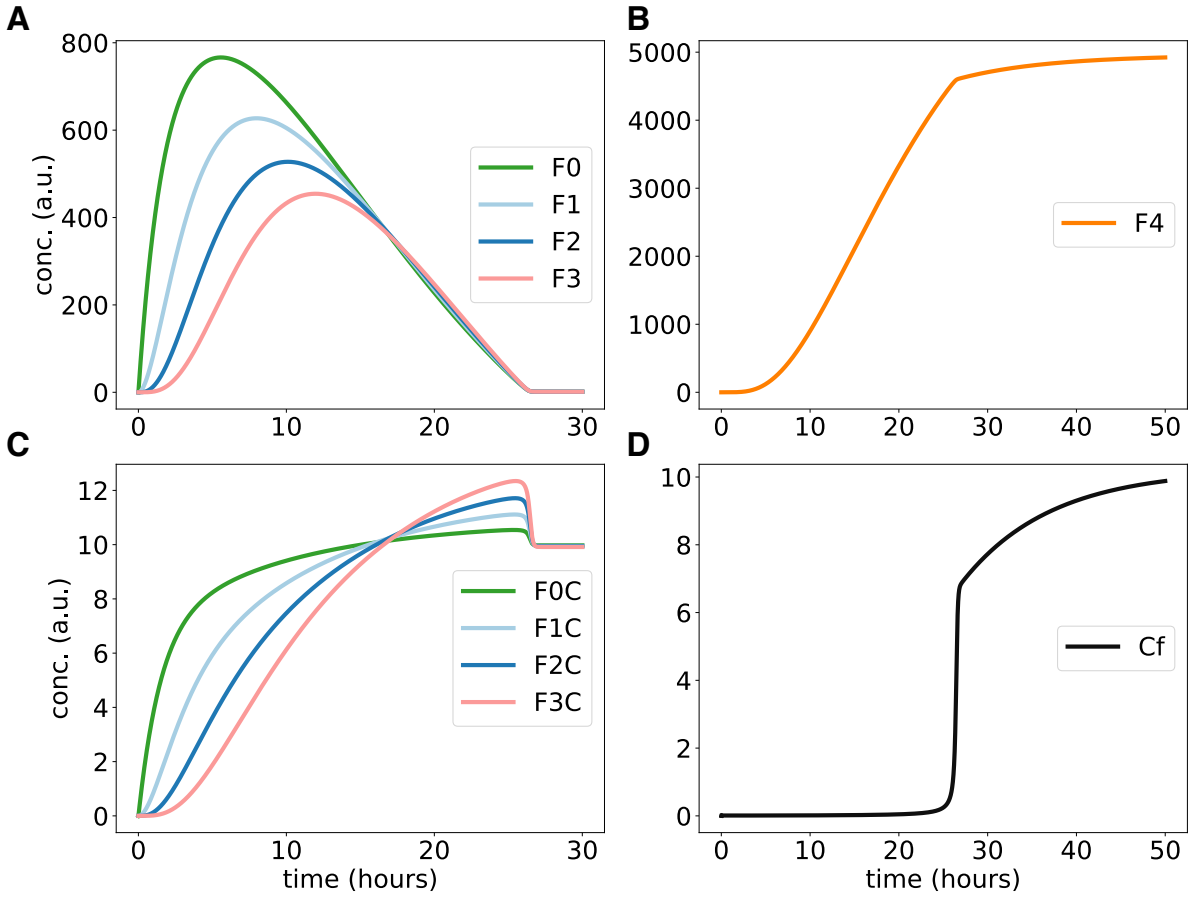

Figure 4. Simulating nonlinear phosphorylations at higher enzyme levels: (A) shows time-courses of phosphorylated FRQ proteins and hyperphosphorylated FRQ (B). Graph (C) shows the concentrations of FRQ-CK1a complexes over time. (D) shows the temporal switch of free kinase Cf after release from sequestration.

2.4. Steady state switches due to increasing enzyme levels

So far, we have characterized in Figs 3 and 4 two specific values of enzyme production Pc (marked by arrows in Fig 5). Fig 5 illustrates that a systematic variation of enzyme levels induces nonlinear dependencies including transitions between different regimes. For low values of Pc we get power-law increases of free kinase (exponent =2.85) and of sequestered protein (exponent = 4.29). Note, that the model contains just bilinear terms. Thus, sequential phosphorylation and sequestration leads to higher exponents as described earlier in other systems [57,61,63]. As discussed above the generation of such input-output switches was studied extensively over the last decades [64–66]. Even though our model can reproduce such nonlinearities,

our focus are temporal switches (compare Figures 1 to 4) relevant for circadian rhythm generation.

Inspecting Fig 5, we find that at Pc = 3 sequestration by increasing FRQ levels flattens the curve of free kinase due to sequestration. Beyond Pc = 4 (white part of the graph) the amount of sequestered protein starts to decline and the release of enzyme leads to more free CK1a.

In summary Fig 5 shows that our nonlinear model generates, in addition to delayed temporal switches and threshold behaviour, interesting nonlinearities of steady states governed by sequestration.

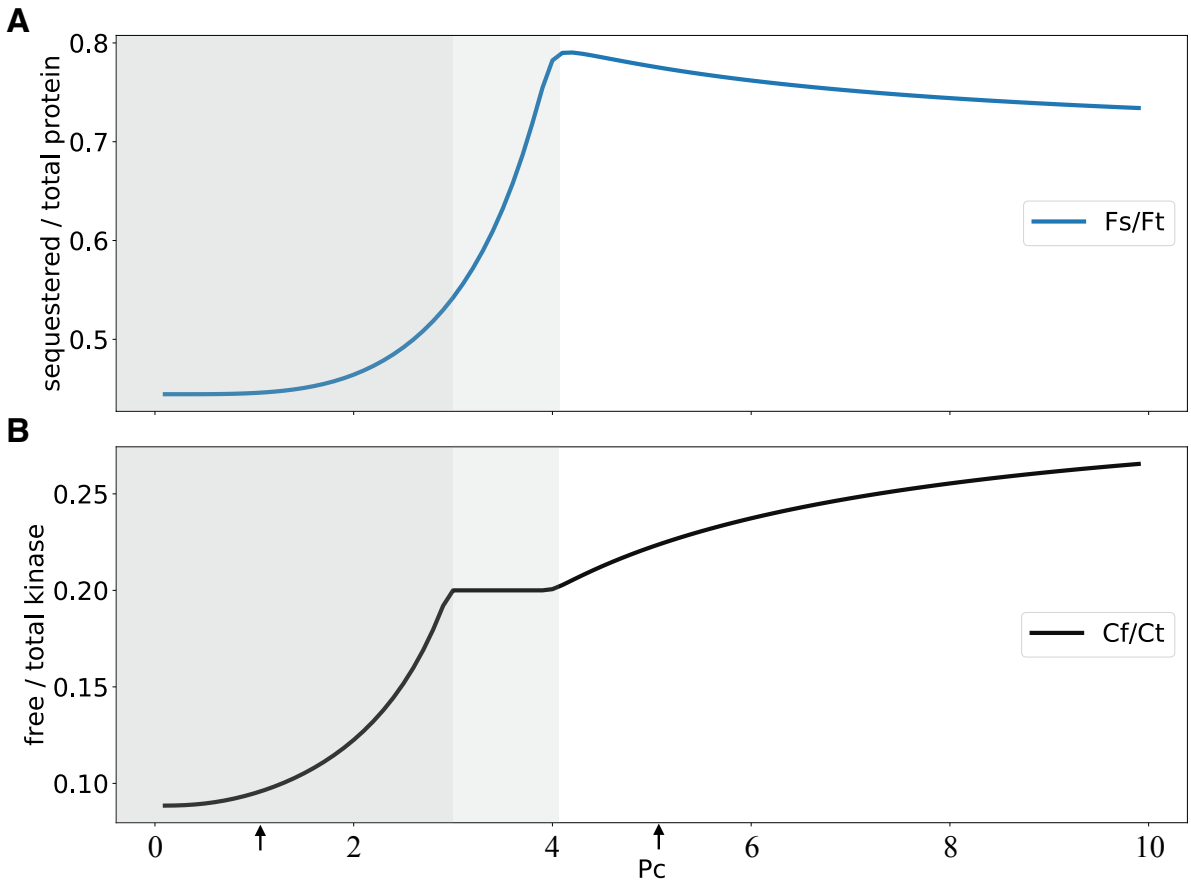

Figure 5. Simulating sequestration based transitions: (A) shows the ratio of sequestered to total FREQUENCY for varying kinase production. (B) shows the ratio of free to total kinase for increasing kinase production.

2.5. Random phosphorylations provide large amplitudes of intermediate phosphorylations

In signaling cascades many phosphorylation sites carry specific functions for activations or complex formations. Up to 100 phosphorylations of intrinsically disordered proteins (IDPs) such as FRQ or PER2 might control cellular processes differently [15]. FRQ proteins have a positively charged N-terminal part and a negatively charged C-terminal part. Initial phosphorylations stabilize whereas hyperphosphorylations favour open conformations by charge repulsion [36]. Thus, the overall number of phosphorylated sites can govern stability, complex formation or nuclear translocation [19,33].

There is some evidence that FRQ is phosphorylated by CK1a in a seemingly random manner [19,53]. The highly flexible FRQ protein forms almost random contacts to the active site of CK1a allowing phosphorylation [67]. Consequently we simulate now instead of processive phosphorylations (compare A1) random phosphorylations as shown in A3. Note, that for up to 100 phosphorylations the number of differently

phosphorylated molecules is astronomically large and exceeds the number of FRQ molecules in a cell and even the number of bacteria on earth [68].

In order to keep simulations with differential equations feasible we introduce new variables F1, F2, etc. These variables lump all FRQ molecules with 1, 2, ... phosphorylations. In other words, Fk represents the $\binom{n}{k}$ molecules with k out of n phosphorylations. These lumped variables seem reasonable since complex formation with FRQ, CK1a, WCC and FRH are influenced by the number of phosphorylations [19]. An overcritical number of phosphorylations destabilizes the FFC complex and makes FRQ accessible to the E3 ligase FWD1 (F-box/WD-40 repeat-containing protein-1) [19,69,70].

Our resulting nonlinear random model (see A4) contains altogether just 2n+2 differential equation making even simulations with n=100 phosphorylations feasible. For a direct comparison with the previous models we show in Fig 6 simulations for n=4. It turns out that the delayed switch with Hill coefficient around 3 are found in these simulations as well (compare A5). Fig 6 displays a new feature of random models - the amplitudes of intermediate states do not decay monotonously. For instance, F1 and F2 have fairly high levels. This property of random models can be traced back to prefactors in the lumped equations. In other words, the combinatorial explosion of molecule types with intermediate phosphorylation numbers enhances the growth of certain Fk levels.

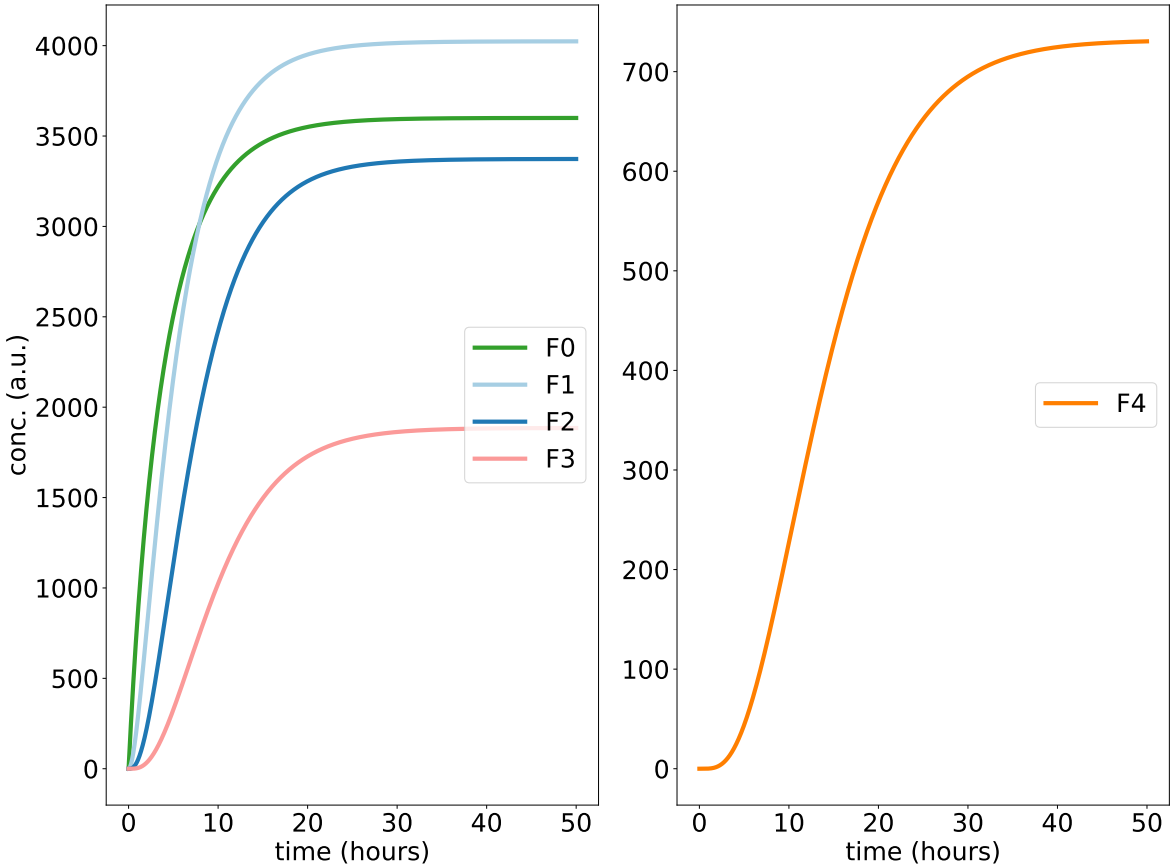

Figure 6. Simulating nonlinear random phosphorylations: Graphs show time-courses of hypo, medium, hyperphosphorylated and fully phosphorylated FRQ proteins for n=4 phosphorylations.

Fig 7 shows representative time-courses of a random model with up to 100 phosphorylations. It turns out that we find delayed temporal switches with high amplitudes in particular at intermediate phosphorylation levels.

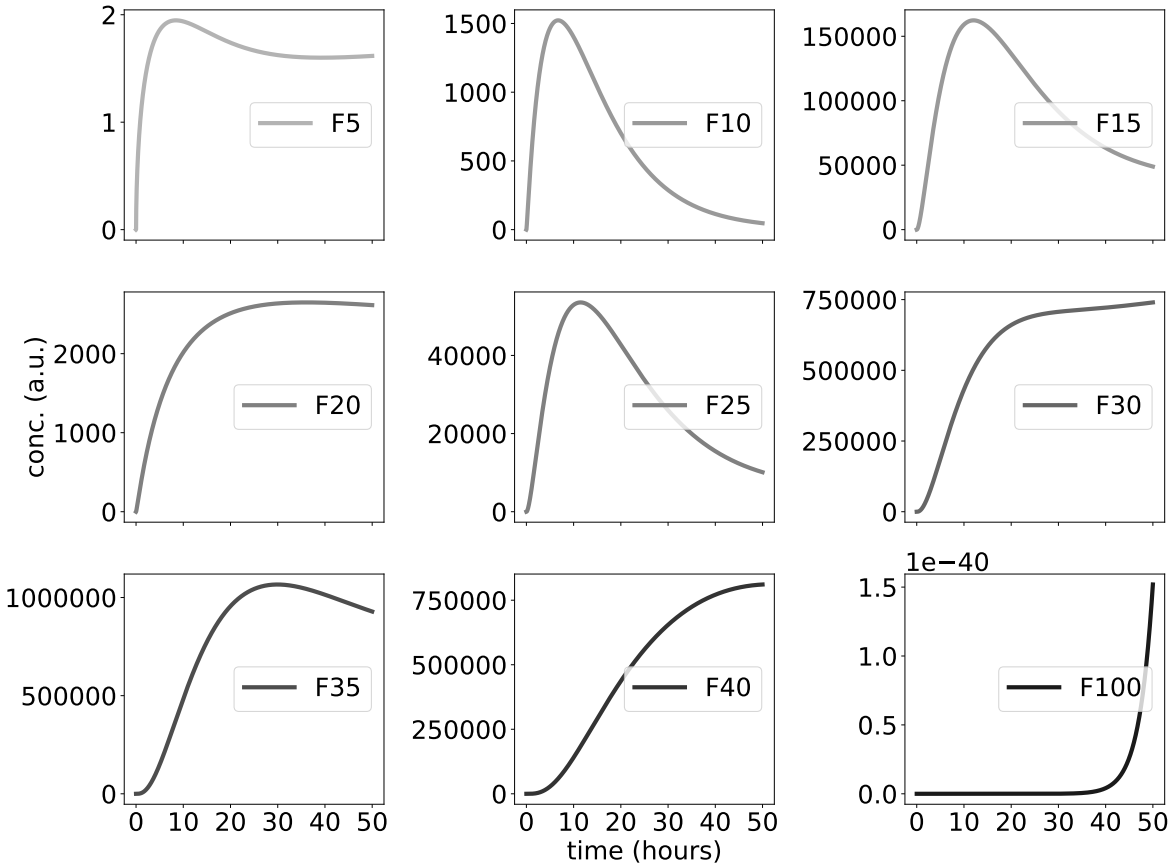

Figure 7. Large-scale simulations of nonlinear, random phosphorylations: Graphs show time-courses of hypo, medium, hyperphosphorylated and fully phosphorylated FRQ proteins for n=100 phosphorylation sites. Note, that the dashed line in Fig 1 (inactivation of FRQ due to phosphorylations) is adapted from 1 – F40 from this figure.

Note, that the widely varying amplitudes can not be directly related to experimental data. Nevertheless, there are generic features of the model that do not depend upon sensitivity to chosen parameter values (compare also Fig 8): hypophosphorylated proteins increase quickly up to medium levels. Levels of medium phosphorylations (F30...F40) exhibit ultrasensitive increases to fairly large amplitudes. Fully phosphorylated proteins are found only at tiny levels.

In Fig 8A we use a logarithmic scale to cover these drastic amplitude differences. The graph reveals that for different parameters intermediate levels of phosphorylations exhibit quite large amplitudes. The steps reflect changes in waveforms (see Fig 7) due to sequestration effects.

In addition to large amplitudes mediators of cellular switches require robust delays and ultrasensitivity. The graphs in Fig 8B and 8C show that intermediate phosphorylation levels obey these properties for different parameters constellations.

In order to test the robustness of these features we analyzed 10-fold reductions of the degradation rate (red) and a 10-fold increase of the enzyme/substrate ratio (green). It turns out that the main properties- huge amplitudes at intermediate phosphorylation levels, long delays, and Hill coefficients above 3- are robust with respect to large parameter variations.

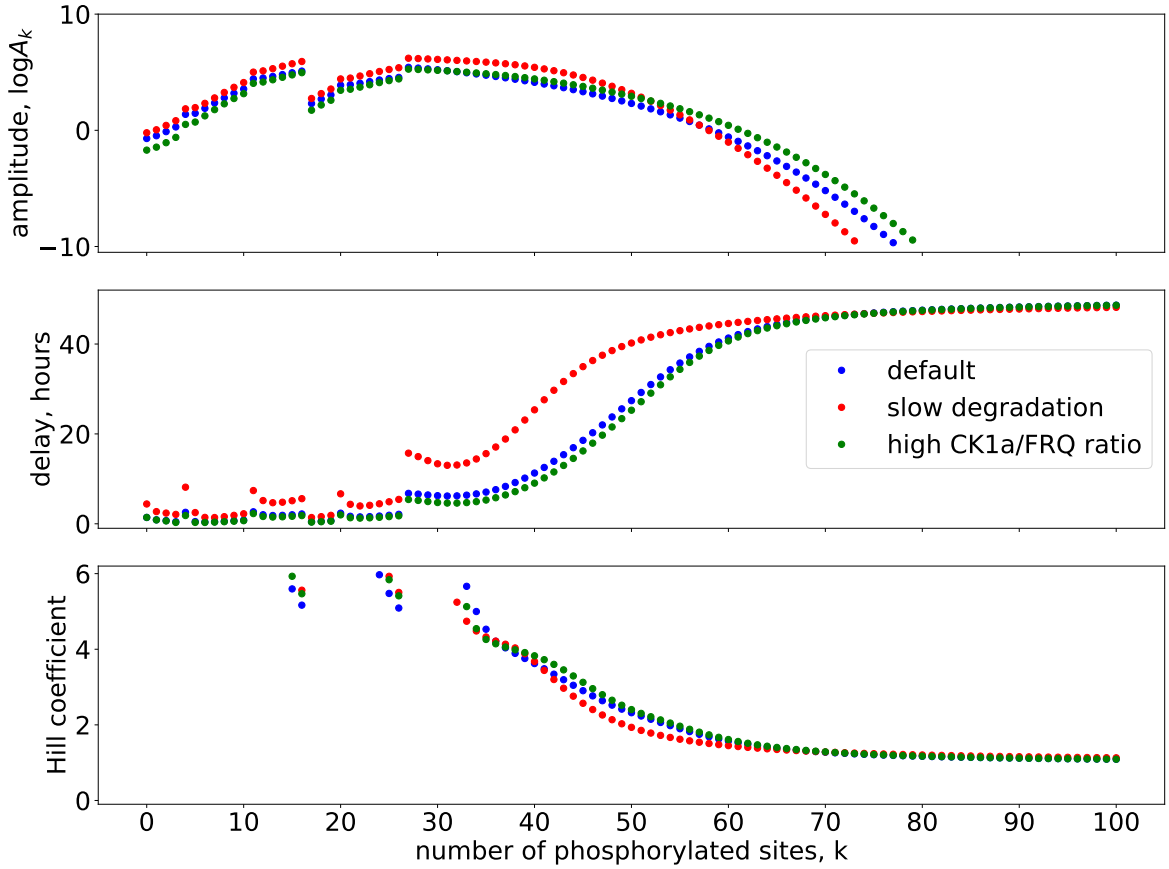

Figure 8. Intermediate phosphorylation levels exhibit large amplitudes, delays and ultrasensitivity: (A) shows log10 values of amplitude for phosphorylated species. (B) depicts delays and (C) shows Hill coefficients for phosphorylated species.

3. Discussion

Self-sustained circadian oscillations require long delays and nonlinearities ("switches") [37,38]. Recent experiments suggest that slow and seemingly random phosphorylations of intrinsically disordered clock proteins control stability and function of clock protein complexes such as FFC in *Neurospora* and PER:CRY in mammals [19,26,71] (A6). Since only few detailed quantitative data are available we compared several generic models describing linear processive phosphorylation, nonlinear distributive phosphorylation, and random phosphorylation. We find that long delays are robustly achieved by long reaction chain lengths and slow degradation (Figures 2 to 4). Sequestration enhances the formation of temporal switches with high Hill coefficients (A5). Thus our simulations support our hypothesis sketched in Fig 1 that multiple random phosphorylation can provide robust delayed switches.

Our theoretical approach is based on a few experimentally observed facts that help to constrain our generic models. Interestingly, most of the data suggest quite similar principles in the *Neurospora* clock and mammalian clocks. In both cases intrinsically disordered proteins (FRQ and PER, respectively) with multiple random phosphorylations are central players within the negative transcriptional-translational feedback loop [22,67,72,73]. Below we focus on the *Neurospora* clock.

The half-life of the FRQ protein is about 3-5 hours [74]. About 100 phosphorylation sites have been identified using isotope labelling and mass spectrometry [29]. The essential priming-independent phosphorylation of non-consensus sites on FRQ by CK1a seems to be slower than 5 sites per hour [55]. Priming by other kinases is relatively fast and appears to be less essential for the principle function of the

core clock. However, other kinases might be relevant for entrainment and temperature compensation not discussed in this paper [19].

Fig 1 illustrates the important role of multiple phosphorylations. FRQ has a positively net charged N-terminal part, a negatively net charged C-terminal part, and a central part involved in proteasomal degradation by FWD1 [36,69,74]. Initial phosphorylation of the C-terminal part early in the circadian day has a stabilizing effect [19,75]. Subsequent phosphorylation of the N-terminal part destabilized the FFC complex allowing degradation. Since charge repulsion governs stability and function, the number of phosphorylations plays a central role.

These experimental findings are reviewed in recent publications [19,24,75] and provide the framework of our models. We do not fit individual parameters to the sparse quantitative data but we adapt the models design to the facts listed above. For example, the number of phosphorylations, the degradation rates, and the central role of CK1a concentration are consistent with the data. Since quantitative details of binding and unbinding of CK1a to FRQ are not known, we simulated two mechanisms: linear processive phosphorylations (A1 and Fig 2) and distributive phosphorylations (A2, A3, Figures 3 to 8). At a first glance, the distributive mechanism seems not consistent with Fig 1 showing a relatively stable FFC complex involving FRQ and CK1a. However, there is evidence that the long intrinsically disordered proteins FRQ binds and unbinds in a seemingly random fashion to the active center of CK1a [36]. Such reoccurring binding events could be simulated by our approach using the distributive mechanism. We start our simulations with zero levels of FRQ protein and enzyme CK1a. This allows to follow the kinetics of complex formations, sequestration, and phosphorylations. In a cell, however, CK1a is present from the beginning. More realistic simulations starting with higher CK1a levels do not change the main results shown in Fig 8.

We emphasize, that our focus on multiple random phosphorylations neglects other essential part of the transcriptional-translational feedback loop (TTFL) modeled in detail elsewhere [27,76–79]. Processes such as nuclear translocation, proteasomal degradation, and epigenetic regulations etc. could be incorporated in future studies. Nevertheless, delayed switch-like behavior due to slow random multiple phosphorylation seems to be central element in circadian rhythm generation. A delayed switch due to multiple phosphorylation is a robust design principle that could be relevant also in other biological systems such as ligand specificity, nuclear import, DNA binding in T-cells [54,80], timing of critical transitions in cell cycle [81], regulation of sleep-wake homeostasis in mice [82], Familial advanced sleep-phase syndrome (FASPS) in humans [25], phototactic sensitivity in green algae [83], and reproductive fitness in cyanobacteria [84].

4. Materials and methods

4.1. Numerics

All the simulations have been performed on a Spyder Python 3.4 platform. Simulations resulting in Figs 1 to 8 have been obtained by numerically solving the ordinary differential equations provided in A1 to A4 via the odeint function from the integrate module of the Scientific Python (SciPy) package with a constant stepsize dt = 0.01 h. The Matplotlib library has been used to generate figures. Codes are available upon request.

4.2. Calculation of Hill coefficients and delays

An ultrasensitive response is often sigmoidal and the curve can be well approximated by the Hill equation. The effective Hill equation is defined for the temporal curves in Figs 2, 3 and 6 (see Equation 1). The effective Hill coefficient n is related to the effective time 90% (ET90) and 10% (ET10) ratio by Equation 2. Here K is the effective time when 50% (or ET50) of total phosphorylation is achieved.

$$Output = \frac{Input^n}{K + Input^n} \tag{1}$$

$$n = \frac{log[81]}{log[ET90/ET10]} \tag{2}$$

Delays are calculated as the time when 50% of the maximal value is achieved for each FRQ species as given in Equation 3.

$$\tau = ET50 \tag{3}$$

4.3. Western blot quantification of FRQ phosphorylations

Experimental details regarding the Western blot in A6 are provided in [52,55]. Western blot images were uploaded in ImageJ software (version 2.0.0-rc-69/1.52p). Each protein band lanes were defined by identical rectangles (60 rows of pixels in width) and for each row the average intensity was extracted. Center of mass and standard deviation of intensities from 60 rows were calculated using normalized density data.

Author Contributions: conceptualization by M.B. and H.H.; methodology by A.U. and H.H.; software by A.U.; validation by A.U. and H.H.; formal analysis by A.U.; investigation, A.U. and H.H.; resources by H.H.; data curation by M.B., D.M. and A.D.; writing—original draft preparation by A.U. and H.H.; writing—review and editing, A.U., H.H., D.M., A.D. and M.B.; visualization by A.U. and H.H.; supervision by M.B. and H.H.; project administration by M.B. and H.H.; funding acquisition by M.B. and H.H.

Funding: This research was funded by the Deutsche Forschungsgemeinschaft (DFG, German Research Foundation) - Project Number 278001972 - TRR 186. We also acknowledge the Open Access Publication Fund of Charité – Universitätsmedizin Berlin.

Acknowledgments: The authors are thankful to Christoph Schmal, Bharath Ananthsubramaniam and Christian H Gabriel for fruitful discussions.

Conflicts of Interest: The authors declare no conflict of interest.

Appendix (Supporting Information)

A

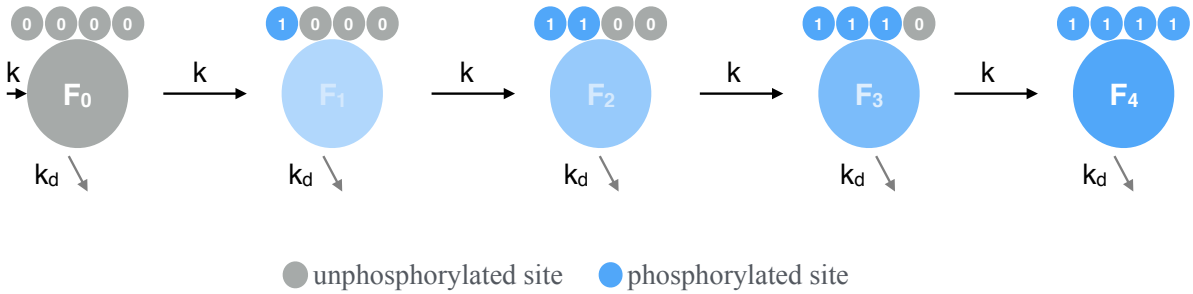

B

$$\frac{d[F_0]}{dt} = k - k * [F_0] - k_d * [F_0]$$
$$\frac{d[F_1]}{dt} = k * [F_0] - k * [F_1] - k_d * [F_1]$$
$$\frac{d[F_2]}{dt} = k * [F_1] - k * [F_2] - k_d * [F_2]$$
$$\frac{d[F_3]}{dt} = k * [F_2] - k * [F_3] - k_d * [F_3]$$
$$\frac{d[F_4]}{dt} = k * [F_3] - k_d * [F_4]$$

Figure A1. (A) Linear model: Schematic diagram of FRQ phosphorylations with turnover of FRQ: FRQ is phosphorylated by CK1a in a sequential processive manner. **(B) Model of up to 4 phosphorylations of FRQ with 5 variables.**

Appendix A.1 Scheme of the linear model, equations and parameters

We modelled the linear phosphorylations using five-variable ordinary differential equations (ODEs). Mass-action kinetics of processive phosphorylations provide long delays shown in Fig 2 with the parameters k=50 and k_d=0.1.

A

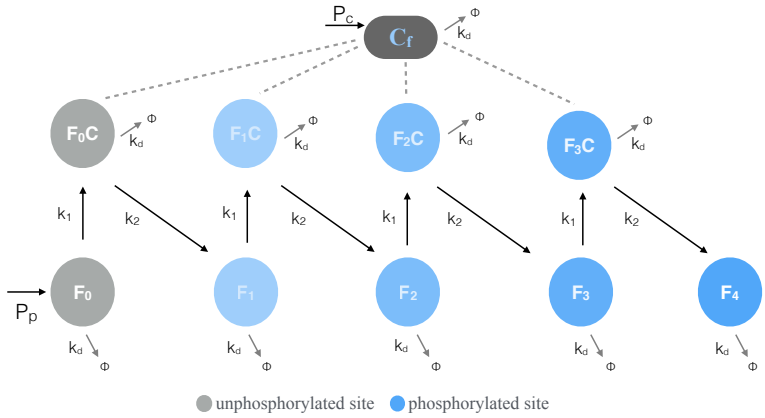

B

$$\frac{d[F_0]}{dt} = P_p - k_1 * [F_0] * [C_f] - k_d * [F_0]$$
$$\frac{d[F_0C]}{dt} = k_1 * [F_0] * [C_f] - k_2 * [F_0C] - k_d * [F_0C]$$
$$\frac{d[F_1]}{dt} = k_2 * [F_0C] - k_1 * [F_1] * [C_f] - k_d * [F_1]$$
$$\frac{d[F_1C]}{dt} = k_1 * [F_1] * [C_f] - k_2 * [F_1C] - k_d * [F_1C]$$
$$\frac{d[F_2]}{dt} = k_2 * [F_1C] - k_1 * [F_2] * [C_f] - k_d * [F_2]$$
$$\frac{d[F_2C]}{dt} = k_1 * [F_2] * [C_f] - k_2 * [F_2C] - k_d * [F_2C]$$
$$\frac{d[F_3]}{dt} = k_2 * [F_2C] - k_1 * [F_3] * [C_f] - k_d * [F_3]$$
$$\frac{d[F_3C]}{dt} = k_1 * [F_3] * [C_f] - k_2 * [F_3C] - k_d * [F_3C]$$
$$\frac{d[F_4]}{dt} = k_2 * [F_3C] - k_d * [F_4]$$

$$\frac{d[C_f]}{dt} = P_c - k_d * [C_f] + (k_2 * [F_0C] + k_2 * [F_1C] + k_2 * [F_2C] + k_2 * [F_3C]) - (k_1 * [F_0] * [C_f] + k_1 * [F_1] * [C_f] + k_1 * [F_2] * [C_f] + k_1 * [F_3] * [C_f])$$

Figure A2. (A) Nonlinear model: Schematic diagram of FRQ phosphorylations with turnover of FRQ and CK1a: FRQ is phosphorylated by CK1a in a sequential distributive manner. **(B) Model of up to 4 phosphorylations of FRQ with 10 variables.**

Appendix A.2 Scheme of the nonlinear model, equations and parameters

We modelled the nonlinear phosphorylations using a ten-variable ODE system. Distributive kinetics of phosphorylations enhances ultrasensitivity shown in Fig 3. Parameters in Figs 3 and 5: k_1=50, k_2=50, k_d=0.1, P_p=500 and P_c=1. Fig 4: P_c=5.

A

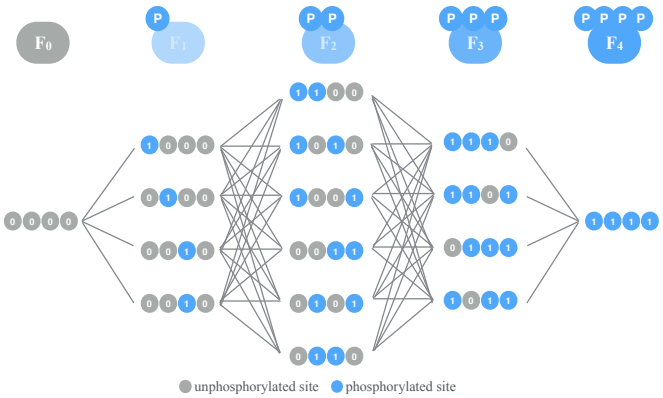

B

$$\frac{d[F_0]}{dt} = P_p - k_1 * [F_0] * [C_f] - k_d * [F_0]$$

$$\frac{d[F_0C]}{dt} = k_1 * [F_0] * [C_f] - k_2 * [F_0C] - k_d * [F_0C]$$

$$\frac{d[F_1]}{dt} = 4 * k_2 * [F_0C] - k_1 * [F_1] * [C_f] - k_d * [F_1]$$

$$\frac{d[F_1C]}{dt} = k_1 * [F_1] * [C_f] - k_2 * [F_1C] - k_d * [F_1C]$$

$$\frac{d[F_2]}{dt} = 3 * k_2 * [F_1C] - k_1 * [F_2] * [C_f] - k_d * [F_2]$$

$$\frac{d[F_2C]}{dt} = k_1 * [F_2] * [C_f] - k_2 * [F_2C] - k_d * [F_2C]$$

$$\frac{d[F_3]}{dt} = 2 * k_2 * [F_2C] - k_1 * [F_3] * [C_f] - k_d * [F_3]$$

$$\frac{d[F_3C]}{dt} = k_1 * [F_3] * [C_f] - k_2 * [F_3C] - k_d * [F_3C]$$

$$\frac{d[F_4]}{dt} = 1 * k_2 * [F_3C] - k_d * [F_4]$$

$$\frac{d[C_f]}{dt} = P_c - k_d * [C_f] + (k_2 * [F_0C] + k_2 * [F_1C] + k_2 * [F_2C] + k_2 * [F_3C]) - (k_1 * [F_0] * [C_f] + k_1 * [F_1] * [C_f] + k_1 * [F_2] * [C_f] + k_1 * [F_3] * [C_f])$$

Figure A3. (A) Nonlinear random model: Schematic diagram of FRQ phosphorylations with turnover of FRQ and CK1a: FRQ is phosphorylated by CK1a in a distributive random manner. **(B) Model of up to n=4 phosphorylations of FRQ.**

Appendix A.3 Noninear random model: scheme, equations and parameters

We modelled the nonlinear random phosphorylations using a ten-variable ODE system. Distributive kinetics and prefactors associated to random phosphorylations together provide large amplitudes of phosphorylations shown in Fig 6. Parameters in Fig 6: k_1=50, k_2=50, k_d=0.1, P_p=500 and P_c=1.

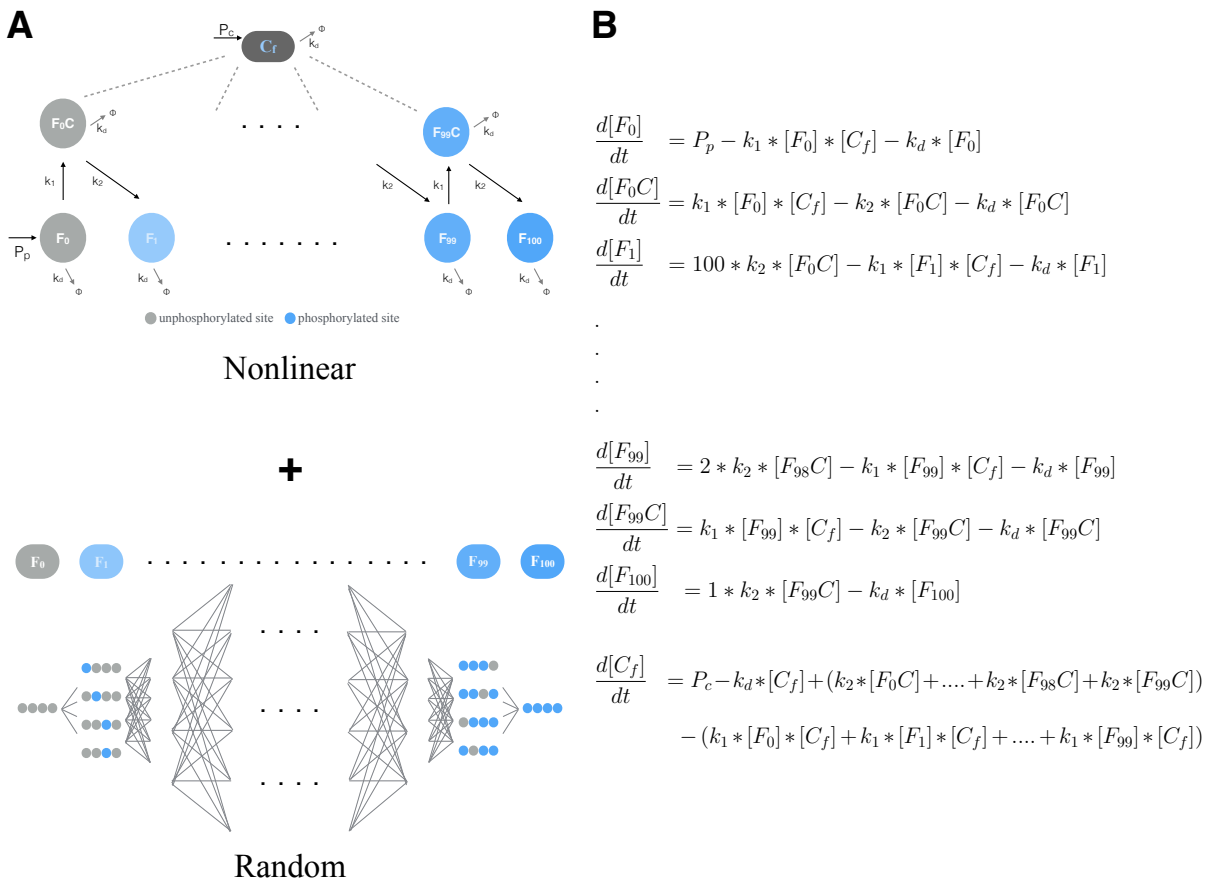

$$\frac{d[F_0]}{dt} = P_p - k_1 * [F_0] * [C_f] - k_d * [F_0]$$
$$\frac{d[F_0C]}{dt} = k_1 * [F_0] * [C_f] - k_2 * [F_0C] - k_d * [F_0C]$$
$$\frac{d[F_1]}{dt} = 100 * k_2 * [F_0C] - k_1 * [F_1] * [C_f] - k_d * [F_1]$$
$$\vdots$$
$$\frac{d[F_{99}]}{dt} = 2 * k_2 * [F_{98}C] - k_1 * [F_{99}] * [C_f] - k_d * [F_{99}]$$
$$\frac{d[F_{99}C]}{dt} = k_1 * [F_{99}] * [C_f] - k_2 * [F_{99}C] - k_d * [F_{99}C]$$
$$\frac{d[F_{100}]}{dt} = 1 * k_2 * [F_{99}C] - k_d * [F_{100}]$$
$$\frac{d[C_f]}{dt} = P_c - k_d * [C_f] + (k_2 * [F_0C] + ... + k_2 * [F_{98}C] + k_2 * [F_{99}C]) - (k_1 * [F_0] * [C_f] + k_1 * [F_1] * [C_f] + ... + k_1 * [F_{99}] * [C_f])$$

Figure A4. (A) Large scale nonlinear random model: Schematic diagram of FRQ phosphorylations with turnover of FRQ and CK1a: FRQ is phosphorylated by CK1a in a distributive random manner. **(B) Model of up to n=100 phosphorylations of FRQ with 2n+2 variables.**

Appendix A.4 Large scale nonlinear random model: scheme, equations and parameters

We modelled the large scale nonlinear random phosphorylations using a 2n+2 (n=100) variable ODE system. Distributive kinetics, prefactors associated to random phosphorylations and longer chain of phosphorylations are shown in Fig 7. Amplitudes, delays and Hill coefficients for 100 phosphorylations shown in Fig 8 are also derived from model simulations. Parameters in Fig 7: k_1=50000, k_2=50000, k_d=1.5, P_p=0.01 and P_c=10. Default (blue) parameters in Fig 8: k_1=50000, k_2=50000, k_d=5, P_p=1 and P_c=10. Slow degradation (red): k_d=0.15 and high CK1a/FRQ ratio (green): P_c=100.

FRQ phospho- -forms	Linear (Figure 2)		Nonlinear (Figure 3)		Nonlinear random (Figure 6)	
	Hill coefficient	*Delay*	*Hill coefficient*	*Delay*	*Hill coefficient*	*Delay*
F0	*1.18*	*2.6*	*1.77*	*1.7*	*1.66*	*2.8*
F1	*1.61*	*6.4*	*2.45*	*4.2*	*2.19*	*4.6*
F2	*1.99*	*10.4*	*2.98*	*6.8*	*2.60*	*6.8*
F3	*2.78*	*14.4*	*3.43*	*9.5*	*2.93*	*9.4*
F4	*3.39*	*18.4*	*3.85*	*14.7*	*3.20*	*13.3*

Figure A5. Hill coefficients and delays: A list of Hill coefficients and time delays of the phosphorylated FRQ across three models. See Figs 2, 3 and 6.

Appendix A.5 Hill coefficients and delays

Hill coefficients and delays are calculated using eqns 1, 2 and 3 for the curves shown in Figs 2, 3 and 6.

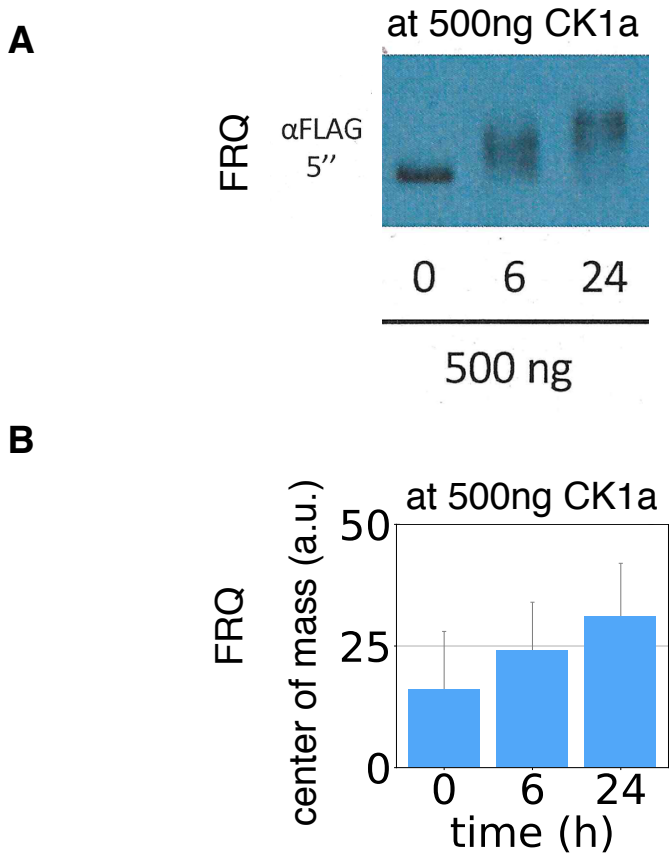

Figure A6. (A) Western blots analysis of FRQ phosphorylations by CK1a: Western blots show the wild-type FRQ phosphorylations at 3 time points (0, 6, 24 hours) [52] (shown with blue dots in Fig 1). **(B) Quantification of phosphorylations:** Western blot image was anlyzed using ImageJ software. Protein bands at 3 time points were surrounded by rectangular boxes. Each rectangular was further divided into 60 equal rows. Expected value and standard deviation of intensities from 60 rows were calculated from the normalized density.

Appendix A.6 Western blot and quantification of FRQ phosphorylations

Experimental data of FRQ phosphorylation indicating multiple slow phosphorylations as sketched in Fig 1. Details are provided in [52,55].

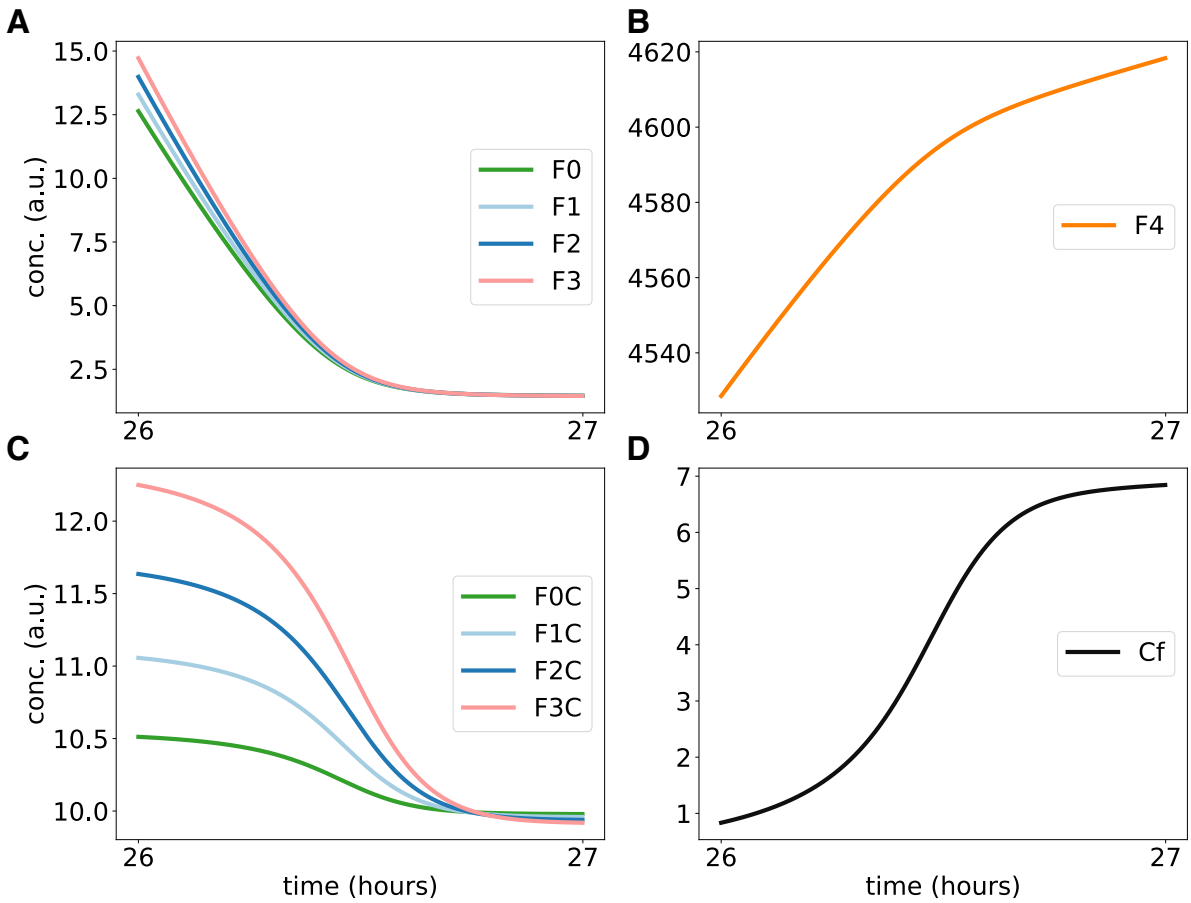

Figure A7. Magnified simulations of nonlinear phosphorylations from Fig 4: Graphs show a one hour time window (26 to 27 hours) and confirm that apparent kinks in Fig 4 are rather smooth curves. The asymptotic equilibrium indicates that most of the FRQ protein is sequestered within complexes.

Appendix A.7 Enlarged time series of nonlinear phosphorylations

References

1. Wever, R. Zum Mechanismus der biologischen 24-Stunden-Periodik. *Kybernetik* **1963**, *2*, 214–231.
2. Konopka, R.J.; Benzer, S. Clock mutants of Drosophila melanogaster. *Proceedings of the National Academy of Sciences* **1971**, *68*, 2112–2116.
3. Nakajima, M.; Imai, K.; Ito, H.; Nishiwaki, T.; Murayama, Y.; Iwasaki, H.; Oyama, T.; Kondo, T. Reconstitution of circadian oscillation of cyanobacterial KaiC phosphorylation in vitro. *Science* **2005**, *308*, 414–415.
4. Mittag, M.; Kiaulehn, S.; Johnson, C.H. The circadian clock in Chlamydomonas reinhardtii. What is it for? What is it similar to? *Plant Physiology* **2005**, *137*, 399–409.
5. Dunlap, J.; Loros, J.; DeCoursey, P. *Chronobiology: biological timekeeping.*; 2004.
6. Bell-Pedersen, D.; Cassone, V.M.; Earnest, D.J.; Golden, S.S.; Hardin, P.E.; Thomas, T.L.; Zoran, M.J. Circadian rhythms from multiple oscillators: lessons from diverse organisms. *Nature Reviews Genetics* **2005**, *6*, 544–556.
7. Relógio, A.; Thomas, P.; Medina-Pérez, P.; Reischl, S.; Bervoets, S.; Gloc, E.; Riemer, P.; Mang-Fatehi, S.; Maier, B.; Schäfer, R.; Leser, U.; Herzel, H.; Kramer, A.; Sers, C. Ras-Mediated Deregulation of the Circadian Clock in Cancer. *PLoS Genetics* **2014**, *10*, e1004338.
8. Dibner, C.; Schibler, U.; Albrecht, U. The mammalian circadian timing system: organization and coordination of central and peripheral clocks. *Annual Review of Physiology* **2010**, *72*, 517–549.
9. Panda, S.; Hogenesch, J.B.; Kay, S.A. Circadian rhythms from flies to human. *Nature* **2002**, *417*, 329–335.
10. Reddy, A.B.; O'Neill, J.S. Healthy clocks, healthy body, healthy mind. *Trends in Cell Biology* **2010**, *20*, 36–44.

11. Hardin, P.E.; Hall, J.C.; Rosbash, M. Feedback of the Drosophila period gene product on circadian cycling of its messenger RNA levels. *Nature* **1990**, *343*, 536–540.
12. Aronson, B.D.; Johnson, K.A.; Loros, J.J.; Dunlap, J.C. Negative feedback defining a circadian clock: autoregulation of the clock gene frequency. *Science* **1994**, *263*, 1578–1584.
13. Duong, H.A.; Robles, M.S.; Knutti, D.; Weitz, C.J. A molecular mechanism for circadian clock negative feedback. *Science* **2011**, *332*, 1436–1439.
14. Brunner, M.; Káldi, K. Interlocked feedback loops of the circadian clock of Neurospora crassa. *Molecular Microbiology* **2008**, *68*, 255–262.
15. Partch, C.L.; Green, C.B.; Takahashi, J.S. Molecular architecture of the mammalian circadian clock. *Trends in Cell Biology* **2014**, *24*, 90–99.
16. Reppert, S.M.; Weaver, D.R. Molecular analysis of mammalian circadian rhythms. *Annual Review of Physiology* **2001**, *63*, 647–676.
17. Hogenesch, J.B.; Chan, W.K.; Jackiw, V.H.; Brown, R.C.; Gu, Y.Z.; Pray-Grant, M.; Perdew, G.H.; Bradfield, C.A. Characterization of a subset of the basic-helix-loop-helix-PAS superfamily that interacts with components of the dioxin signaling pathway. *Journal of Biological Chemistry* **1997**, *272*, 8581–8593.
18. Brown, S.A.; Kowalska, E.; Dallmann, R. (Re) inventing the circadian feedback loop. *Developmental Cell* **2012**, *22*, 477–487.
19. Diernfellner, A.C.; Brunner, M. Phosphorylation Timers in the Neurospora crassa Circadian Clock. *Journal of Molecular Biology* **2020**. doi:10.1016/j.jmb.2020.04.004.
20. Lee, C.; Etchegaray, J.P.; Cagampang, F.R.; Loudon, A.S.; Reppert, S.M. Posttranslational mechanisms regulate the mammalian circadian clock. *Cell* **2001**, *107*, 855–867.
21. Narasimamurthy, R.; Hunt, S.; Lu, Y.; Fustin, J.; Okamura, H.; Partch, C.; Forger, D.; Kim, J.; Virshup, D. CK1δ/ϵ protein kinase primes the PER2 circadian phosphoswitch. *Proceedings of the National Academy of Sciences* **2018**, *115*, 5986–5991.
22. Gallego, M.; Virshup, D.M. Post-translational modifications regulate the ticking of the circadian clock. *Nature Reviews Molecular Cell Biology* **2007**, *8*, 139–148.
23. Sancar, G.; Sancar, C.; Brunner, M.; Schafmeier, T. Activity of the circadian transcription factor White Collar Complex is modulated by phosphorylation of SP-motifs. *FEBS Letters* **2009**, *583*, 1833–1840.
24. Wang, B.; Kettenbach, A.N.; Zhou, X.; Loros, J.J.; Dunlap, J.C. The phospho-code determining circadian feedback loop closure and output in Neurospora. *Molecular Cell* **2019**, *74*, 771–784.
25. Vanselow, K.; Vanselow, J.T.; Westermark, P.O.; Reischl, S.; Maier, B.; Korte, T.; Herrmann, A.; Herzel, H.; Schlosser, A.; Kramer, A. Differential effects of PER2 phosphorylation: molecular basis for the human familial advanced sleep phase syndrome (FASPS). *Genes & Development* **2006**, *20*, 2660–2672.
26. Aryal, R.P.; Kwak, P.B.; Tamayo, A.G.; Gebert, M.; Chiu, P.L.; Walz, T.; Weitz, C.J. Macromolecular assemblies of the mammalian circadian clock. *Molecular Cell* **2017**, *67*, 770–782.
27. Upadhyay, A.; Brunner, M.; Herzel, H. An inactivation switch enables rhythms in a Neurospora clock model. *International Journal of Molecular Sciences* **2019**, *20*, 2985.
28. Schafmeier, T.; Haase, A.; Káldi, K.; Scholz, J.; Fuchs, M.; Brunner, M. Transcriptional feedback of Neurospora circadian clock gene by phosphorylation-dependent inactivation of its transcription factor. *Cell* **2005**, *122*, 235–246.
29. Tang, C.T.; Li, S.; Long, C.; Cha, J.; Huang, G.; Li, L.; Chen, S.; Liu, Y. Setting the pace of the Neurospora circadian clock by multiple independent FRQ phosphorylation events. *Proceedings of the National Academy of Sciences* **2009**, *106*, 10722–10727.
30. Merrow, M.; Brunner, M.; Roenneberg, T. Assignment of circadian function for the Neurospora clock gene frequency. *Nature* **1999**, *399*, 584.
31. Loros, J.J.; Dunlap, J.C. Genetic and molecular analysis of circadian rhythms in Neurospora. *Annual Review of Physiology* **2001**, *63*, 757–794.
32. Tataroglu, O.; Schafmeier, T. Of switches and hourglasses: regulation of subcellular traffic in circadian clocks by phosphorylation. *EMBO Reports* **2010**, *11*, 927–935.
33. Diernfellner, A.; Schafmeier, T. Phosphorylations: Making the Neurosporacrassa circadian clock tick. *FEBS Letters* **2011**, *585*, 1461–1466.
34. Lauinger, L.; Diernfellner, A.; Falk, S.; Brunner, M. The RNA helicase FRH is an ATP-dependent regulator of CK1a in the circadian clock of Neurospora crassa. *Nature Communications* **2014**, *5*, 3598.

35. Schafmeier, T.; Káldi, K.; Diernfellner, A.; Mohr, C.; Brunner, M. Phosphorylation-dependent maturation of Neurospora circadian clock protein from a nuclear repressor toward a cytoplasmic activator. *Genes and Development* **2006**, *20*, 297–306.
36. Querfurth, C.; Diernfellner, A.; Gin, E.; Malzahn, E.; Höfer, T.; Brunner, M. Circadian conformational change of the Neurospora clock protein FREQUENCY triggered by clustered hyperphosphorylation of a basic domain. *Molecular Cell* **2011**, *43*, 713–722.
37. Glass, L.; Mackey, M.C. *From Clocks to Chaos: The Rhythms of Life*; Princeton University Press, 1988.
38. Korenčič, A.; Bordyugov, G.; Košir, R.; Rozman, D.; Goličnik, M.; Herzel, H. The interplay of cis-regulatory elements rules circadian rhythms in mouse liver. *PloS One* **2012**, *7*.
39. Bordyugov, G.; Westermark, P.O.; Korenčič, A.; Bernard, S.; Herzel, H. Mathematical Modeling in Chronobiology. In *Springer, Berlin, Heidelberg*; 2013; pp. 335–357.
40. MacDonald, N. *Biological delay systems: linear stability theory*; Cambridge University Press, 2008.
41. Bernard, S.; Čajavec, B.; Pujo-Menjouet, L.; Mackey, M.C.; Herzel, H. Modelling transcriptional feedback loops: the role of Gro/TLE1 in Hes1 oscillations. *Philosophical Transactions of the Royal Society A: Mathematical, Physical and Engineering Sciences* **2006**, *364*, 1155–1170.
42. Aulehla, A.; Pourquie, O. Oscillating signaling pathways during embryonic development. *Current Opinion in Cell Biology* **2008**, *20*, 632–637.
43. Hoffmann, A.; Levchenko, A.; Scott, M.L.; Baltimore, D. The IκB-NF-κB signaling module: temporal control and selective gene activation. *Science* **2002**, *298*, 1241–1245.
44. Ashall, L.; Horton, C.A.; Nelson, D.E.; Paszek, P.; Harper, C.V.; Sillitoe, K.; Ryan, S.; Spiller, D.G.; Unitt, J.F.; Broomhead, D.S.; Kell, D.B.; Rand, D.A.; Sée1, V.; White, M.R.H. Pulsatile stimulation determines timing and specificity of NF-κB-dependent transcription. *Science* **2009**, *324*, 242–246.
45. Purvis, J.E.; Karhohs, K.W.; Mock, C.; Batchelor, E.; Loewer, A.; Lahav, G. p53 dynamics control cell fate. *Science* **2012**, *336*, 1440–1444.
46. Diernfellner, A.; Querfurth, C.; Salazar, C.; Höfer, T.; Brunner, M. Phosphorylation modulates rapid nucleocytoplasmic shuttling and cytoplasmic accumulation of Neurospora clock protein FRQ on a circadian time scale. *Genes & Development* **2009**, *23*, 2192–2200.
47. Toh, K.L.; Jones, C.R.; He, Y.; Eide, E.J.; Hinz, W.A.; Virshup, D.M.; Ptáček, L.J.; Fu, Y.H. An hPer2 phosphorylation site mutation in familial advanced sleep phase syndrome. *Science* **2001**, *291*, 1040–1043.
48. Griffith, J. Mathematics of cellular control processes I. Negative feedback to one gene. *Journal of Theoretical Biology* **1968**, *20*, 202–208.
49. Ananthasubramaniam, B.; Herzel, H. Positive feedback promotes oscillations in negative feedback loops. *PLoS One* **2014**, *9*, e104761.
50. Goodwin, B.C. Oscillatory behavior in enzymatic control processes. *Advances in Enzyme Regulation* **1965**, *3*, 425–438.
51. Gonze, D.; Ruoff, P. The Goodwin Oscillator and its Legacy. *Acta Biotheoretica* **2020**, pp. 1–18.
52. Marzoll, D. *The Role of Neurospora Casein Kinase 1a in Circadian Timekeeping.*; PhD dissertation Heidelberg University, 2019.
53. Baker, C.L.; Kettenbach, A.N.; Loros, J.J.; Gerber, S.A.; Dunlap, J.C. Quantitative proteomics reveals a dynamic interactome and phase-specific phosphorylation in the Neurospora circadian clock. *Molecular Cell* **2009**, *34*, 354–363.
54. Salazar, C.; Höfer, T. Multisite protein phosphorylation–from molecular mechanisms to kinetic models. *The FEBS Journal* **2009**, *276*, 3177–3198.
55. Diernfellner, A.C.; Lauinger, L.; Shostak, A.; Brunner, M. A pathway linking translation stress to checkpoint kinase 2 signaling in Neurospora crassa. *Proceedings of the National Academy of Sciences* **2019**, *116*, 17271–17279.
56. Ferrell, J.E.; Ha, S.H.; others. Ultrasensitivity part II: multisite phosphorylation, stoichiometric inhibitors, and positive feedback. *Trends in Biochemical Sciences* **2014**, *39*, 556–569.
57. Legewie, S.; Schoeberl, B.; Blüthgen, N.; Herzel, H. Competing docking interactions can bring about bistability in the MAPK cascade. *Biophysical Journal* **2007**, *93*, 2279–2288.
58. Klipp, E.; Liebermeister, W.; Wierling, C.; Kowald, A. *Systems biology : a textbook*, 2. ed.; Wiley-Blackwell, 2016.
59. Kim, J.K. Mathematical Modeling and Analysis of Cellular Clocks. *Ph.D. Thesis, University of Michigan* **2013**.
60. Ingalls, B. *Mathematical modeling in systems biology: an introduction*; MIT Press, 2013.

61. Ferrell, J.E.; Ha, S.H. Ultrasensitivity part I: Michaelian responses and zero-order ultrasensitivity. *Trends in Biochemical Sciences* **2014**, *39*, 496–503.
62. Legewie, S.; Blüthgen, N.; Herzel, H. Quantitative analysis of ultrasensitive responses. *FEBS Journal* **2005**, *272*, 4071–4079.
63. Clodong, S.; Dühring, U.; Kronk, L.; Wilde, A.; Axmann, I.; Herzel, H.; Kollmann, M. Functioning and robustness of a bacterial circadian clock. *Molecular Systems Biology* **2007**, *3*.
64. Thomson, M.; Gunawardena, J. Unlimited multistability in multisite phosphorylation systems. *Nature* **2009**, *460*, 274–277.
65. Blüthgen, N.; Bruggeman, F.J.; Legewie, S.; Herzel, H.; Westerhoff, H.V.; Kholodenko, B.N. Effects of sequestration on signal transduction cascades. *The FEBS Journal* **2006**, *273*, 895–906.
66. Legewie, S.; Blüthgen, N.; Schäfer, R.; Herzel, H. Ultrasensitization: switch-like regulation of cellular signaling by transcriptional induction. *PLoS Computational Biology* **2005**, *1*.
67. Querfurth, C.; Diernfellner, A.; Heise, F.; Lauinger, L.; Neiss, A.; Tataroglu, Ö.; Brunner, M.; Schafmeier, T. Posttranslational regulation of Neurospora circadian clock by CK1a-dependent phosphorylation. Cold Spring Harbor Laboratory Press, 2007, Vol. 72, pp. 177–183.
68. Whitman, W.B.; Coleman, D.C.; Wiebe, W.J. Prokaryotes: the unseen majority. *Proceedings of the National Academy of Sciences* **1998**, *95*, 6578–6583.
69. He, Q.; Cheng, P.; Yang, Y.; He, Q.; Yu, H.; Liu, Y. FWD1-mediated degradation of FREQUENCY in Neurospora establishes a conserved mechanism for circadian clock regulation. *The EMBO Journal* **2003**, *22*, 4421–4430.
70. Larrondo, L.F.; Olivares-Yañez, C.; Baker, C.L.; Loros, J.J.; Dunlap, J.C. Decoupling circadian clock protein turnover from circadian period determination. *Science* **2015**, *347*, 1257277–1257277.
71. Philpott, J.M.; Narasimamurthy, R.; Ricci, C.G.; Freeberg, A.M.; Hunt, S.R.; Yee, L.E.; Pelofsky, R.S.; Tripathi, S.; Virshup, D.M.; Partch, C.L. Casein kinase 1 dynamics underlie substrate selectivity and the PER2 circadian phosphoswitch. *Elife* **2020**, *9*, e52343.
72. Hurley, J.M.; Larrondo, L.F.; Loros, J.J.; Dunlap, J.C. Conserved RNA helicase FRH acts nonenzymatically to support the intrinsically disordered neurospora clock protein FRQ. *Molecular Cell* **2013**, *52*, 832–843.
73. Schlosser, A.; Vanselow, J.T.; Kramer, A. Mapping of phosphorylation sites by a multi-protease approach with specific phosphopeptide enrichment and nanoLC- MS/MS analysis. *Analytical Chemistry* **2005**, *77*, 5243–5250.
74. Görl, M.; Merrow, M.; Huttner, B.; Johnson, J.; Roenneberg, T.; Brunner, M. A PEST-like element in FREQUENCY determines the length of the circadian period in Neurospora crassa. *The EMBO Journal* **2001**, *20*, 7074–7084.
75. Liu, X.; Chen, A.; Caicedo-Casso, A.; Cui, G.; Du, M.; He, Q.; Lim, S.; Kim, H.J.; Hong, C.I.; Liu, Y. FRQ-CK1 interaction determines the period of circadian rhythms in Neurospora. *Nature Communications* **2019**, *10*, 1–13.
76. Gonze, D.; Leloup, J.c.; Goldbeter, A. Theoretical models for circadian rhythms in Neurospora and Drosophila. *Comptes Rendus de l'Académie des Sciences-Series III-Sciences de la Vie* **2000**, *323*, 57–67.
77. Ruoff, P.; Loros, J.J.; Dunlap, J.C. The relationship between FRQ-protein stability and temperature compensation in the Neurospora circadian clock. *Proceedings of the National Academy of Sciences* **2005**, *102*, 17681–17686.
78. P François. A model for the Neurospora circadian clock. *Biophysical Journal* **2005**, *88*, 2369–2383.
79. Hong, C.I.; Jolma, I.W.; Loros, J.J.; Dunlap, J.C.; Ruoff, P. Simulating dark expressions and interactions of frq and wc-1 in the Neurospora circadian clock. *Biophysical Journal* **2008**, *94*, 1221–1232.
80. Gabriel, C.H.; Gross, F.; Karl, M.; Stephanowitz, H.; Hennig, A.F.; Weber, M.; Gryzik, S.; Bachmann, I.; Hecklau, K.; Wienands, J.; Schuchhardt, J.; Herzel, H.; Radbruch, A.; Krause, E.; Baumgrass, R. Identification of novel nuclear factor of activated T cell (NFAT)-associated proteins in T cells. *Journal of Biological Chemistry* **2016**, *291*, 24172–24187.
81. Deshaies, R.J.; Ferrell Jr, J.E. Multisite phosphorylation and the countdown to S phase. *Cell* **2001**, *107*, 819–822.
82. Brüning, F.; Noya, S.B.; Bange, T.; Koutsouli, S.; Rudolph, J.D.; Tyagarajan, S.K.; Cox, J.; Mann, M.; Brown, S.A.; Robles, M.S. Sleep-wake cycles drive daily dynamics of synaptic phosphorylation. *Science* **2019**, *366*, 3617.
83. Böhm, M.; Boness, D.; Fantisch, E.; Erhard, H.; Frauenholz, J.; Kowalzyk, Z.; Marcinkowski, N.; Kateriya, S.; Hegemann, P.; Kreimer, G. Channelrhodopsin-1 Phosphorylation Changes with Phototactic Behavior and Responds to Physiological Stimuli in Chlamydomonas. *The Plant Cell* **2019**, *31*, 886–910.
84. Ouyang, Y.; Andersson, C.R.; Kondo, T.; Golden, S.S.; Johnson, C.H. Resonating circadian clocks enhance fitness in cyanobacteria. *Proceedings of the National Academy of Sciences* **1998**, *95*, 8660–8664.

© 2020 by the authors. Submitted to *Journal Not Specified* for possible open access publication under the terms and conditions of the Creative Commons Attribution (CC BY) license (http://creativecommons.org/licenses/by/4.0/).